CHEMICAL ENGINEERING TRANSACTIONS
VOL. 57, 2017
A publication of AIDIC
The Italian Association of Chemical Engineering
Online at www.aidic.it/cet
Guest Editors: Sauro Pierucci, Jiří Jaromír Klemeš, Laura Piazza, Serafim Bakalis

ISBN978-88-95608- 48-8; **ISSN** 2283-9216
DOI: 10.3303/CET1757206

Cavitations Phenomenon in T-mixer with Exocentric Inputs

Khaled Oualha, Mounir Ben Amar, Armelle Michau, Andrei Kanaev

Laboratoire des Sciences des Procédés et des Matériaux, CNRS, Université Paris 13, Sorbonne Paris Cité, 99 avenue J.-B. Clément, 93430, Villetaneuse, France
mounir.benamar@lspm.cnrs.fr.

In this paper, static light scattering (SLS) measurements were carried out in a turbulent water flow in a T-mixer and the cavitation phenomenon was detected from a certain flow rate correspondent to Re = 7500. The occurrence of this phenomenon is validated by computational fluid dynamics (CFD) simulations using Fluent Software V.15.0, of velocity and pressure in the flow. The simulation results show that there is a large drop of pressure in the zone of the impact of the inlet fluids, which can attain that of the water vapor, thus creating conditions for nucleation of bubbles.
Keywords: T-mixer, water flow, cavitation, light scattering.

1. Introduction

The phenomenon of cavitation is highlighted by Osborne Reynolds in 1894 (Reynolds et al., 1894), it is a general phenomenon of fluid flows in encountering an obstacle. The phenomenon of cavitation in water can be present in many practical processes, such as boat propellers, pressure reducing valves, or even vortex diodes for water streams disinfection (Ranade et al., 2015; 2016). According to Knapp (Knapp et al., 1970), Cavitation can be classified into several different regimes and in each case the occurrence of cavitations occurs by acceleration accompanied by a large drop in pressure at a given point in the cavity. This causes the formation of vapor bubbles. The bubbles move downstream until the pressure increases and forces the bubbles to collapse. We suggest monitoring the appearance of this sudden perturbation of a fluid (cavitation) in strongly turbulent flows by an increase of the scattered light intensity due to the refraction change on the interface between liquid and vapor phases.
The turbulent flow is established in a T-mixer at sufficiently high Reynolds numbers above 500, as reported in many studies devoted to the flow dynamics and particles precipitation in T-mixers (Schwarzer and Peukert, 2004, Marchisio et al., 2006, Gradl et al., 2006) and consequences on the nanoparticles preparation (Hosni et al., 2015). For sufficiently rapid reactions characteristic of the sol-gel process, Re = 4500-6000 have been applied to achieve homogeneous “point-like” reaction conditions (Rivallin et al., 2005; Azouani et al., 2010), which permitted to generate macroscopic samples of size-selected TiO_2 and ZrO_2 nanoparticles (Azouani et al., 2007a, Azouani et al., 2007b; Labidi et al., 2015).
The phenomenon of cavitation has never been observed in T mixers of chemical reactors. On the other hand, it can affect the solid precipitation dynamics and produced materials. The objective of this work is to characterize the cavitation phenomenon in T-mixer by using SLS measurements and numerical simulation.

2. Experimental study

The T-mixer used in the present work is shown in (Figure 1) It contains two exocentric input arms with diameter 1 mm and the output tube with the diameter 2 mm in order to conserve the Reynolds number. In order to for a vortex, the symmetry axes of two input arms are shifted by 1 mm. The coordinate frame is fixed to have y and z axes respectively along the input and output flow directions. The mixer is made of transparent material (glass), which enables optical measurements in the fluid flow

Please cite this article as: Oualha K., Ben Amar M., Michau A., Kanaev A., 2017, Cavitation phenomenon in t-mixer with exocentric inputs, Chemical Engineering Transactions, 57, 1231-1236 DOI: 10.3303/CET1757206

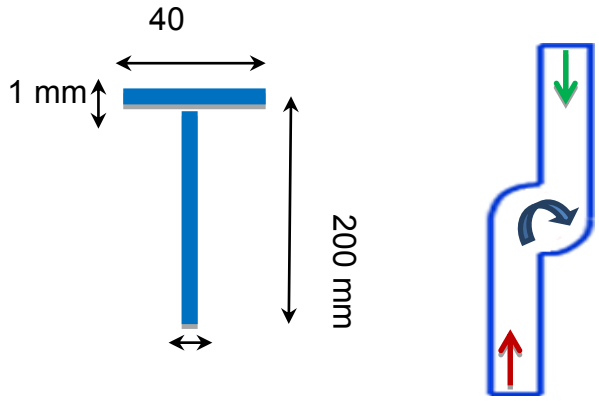

Figure 1: Schema of the micro T-mixer

The light scattering measurements were performed in a light of 40 mW / 640 nm single-frequency laser Cube 640-40 Circular (Coherent) using two monomode optical fibres placed at 3 mm distance to the symmetry axis of the output tube. One fibre (emitting) conducts the laser light to the sample and another one receives the scattered photons at a right angle to the incident light for the analysis. The observation volume ~$3 \cdot 10^{-4}$ cm^3 with characteristic length ~300 μm (1/6 of the output tube diameter) is sufficiently small to avoid multiple scattering events. The single photon analysis was performed with a 16-bit, 255 channels PC board plugged digital photon-correlator (PhotoCor Instruments).
Two images of the T-mixer with the fluid flows correspondent to Reynolds numbers 6000 and 7500 ($Re=4Q\rho/\pi\eta d$, where Q, ρ, and η are the fluid flow rate, mass density and dynamic viscosity of the flow) are shown in (Figure 2) It shows a cleat appearance of a mass density change due to liquid-vapor phase transition in the fluid. We assign this phenomenon to cavitation, which accounts for the liquid boiling triggered by the static pressure decrease down to the vapor pressure (P_{vap}).

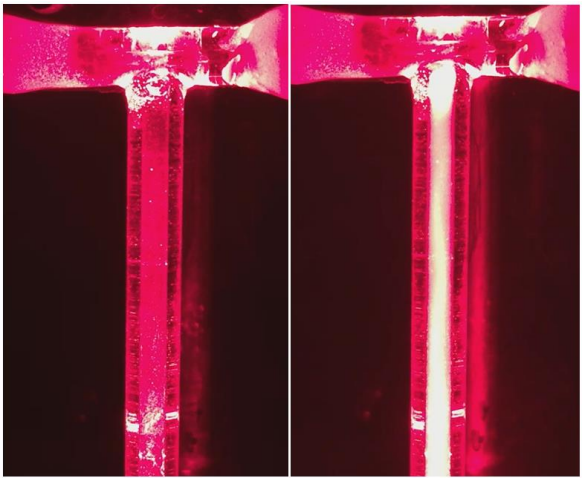

Figure 2: Light scattering (633 nm) images of the exocentric T mixer during water injection (20°C) with Re numbers 6000 (a) and 7500 (b).

In the case of a monophasic flow, it is not expected to have any strong scattering of light, because of the liquid incompressibility (ρ = constant). Accordingly, no scattered light was observed on out T-mixer at moderate and low Re < 7500. On the other hand, when the flow rate becomes Q ≥ 0.75 L / min (Re ≥ 7500), there is a strong perturbation of the water flow in the outlet tube of the T-mixer. At this point of Re = 7500, there is the creation of a liquid-vapor interface that allows the diffusion of light (Figure 3).

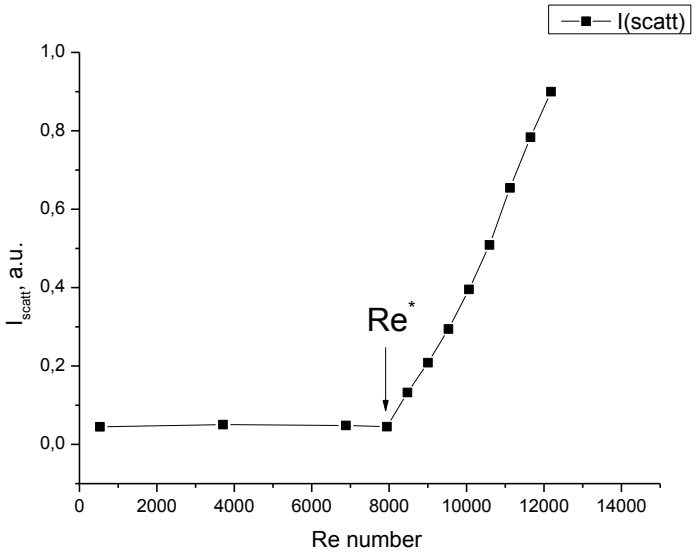

Figure 3: Evolution of scattered light as a function of Reynolds number

3. Numerical study

3.1 Geometry et meshing

To validate, numerically, our experimental observation of the cavitations we use CFD (Computational Fluid Dynamics) and Fluent software. During the last year, the work concerning the simulation of cavitation (Salvador et al., 2007; Gavaises et al., 2015) has increased due to the availability of commercial codes, which allowed developing robust models and the ability to run the code on PC. Numerous studies (Cerutti et al., 2000; Singhal et al., 2002) have contributed to the improvement of CFD models of cavitation to obtain more realistic approach to simulate steam formation, which makes it possible to predict the zones most affected in the experimental device by the phenomenon of cavitation.
The T-mix in (Figure 4) is consisting of two injection arms, each with an internal diameter of 1 mm and a length of 20 mm, and an outlet leg with an internal diameter of 2 mm and a Length of 200 mm. The diameters were chosen to conserve the same Reynolds number.

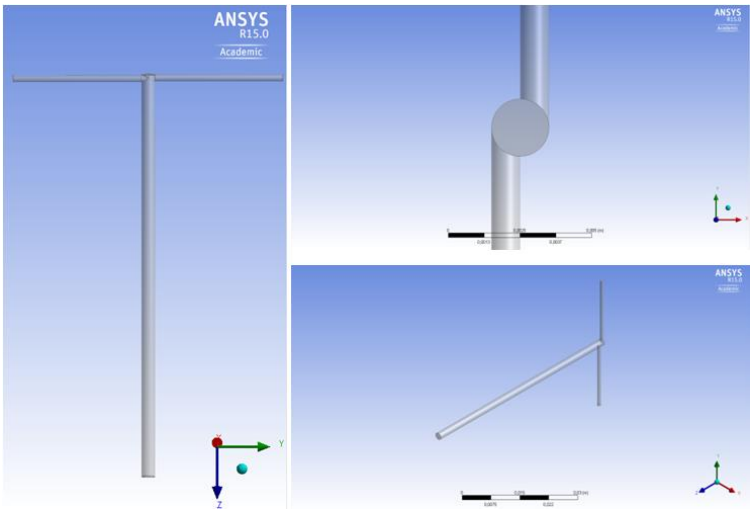

Figure 4: Geometry of the T-mixer

After having drawn the T-mixer, we proceed to its mesh (Figure 5). The mesh is optimized, in term of time and calculation precision, for our geometry (300 000 elements) with a finer mesh in sensitive zones.

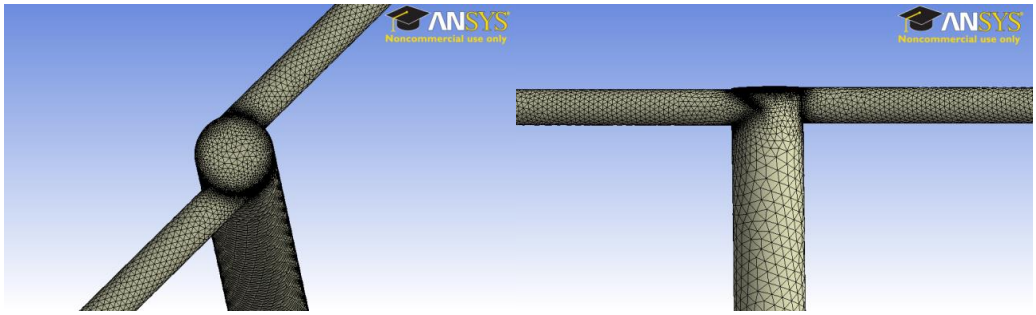

Figure 5: meshing of the T-mixer

3.2 Numerical Setup

Our flow is considered as a turbulent flow with an incompressible Newtonian fluid in the microchannels, thus generally described by the mean Navier-Stokes equation and the continuity equation Eq (1).
Of all the turbulence models, the k-ε model (Launder et al., 1972) is the most widely used in the literature and trade codes such as Fluent. For an incompressible Newtonian fluid, two transport equations are solved: k (the kinetic energy of turbulence) and ε (the dissipation of turbulence). It remains to determine k and ε with the two respective transport equations Eq (6) and Eq (7):

$$\begin{cases} \dfrac{\partial \langle u_i \rangle}{\partial t} + \dfrac{\partial \langle u_j \, 'u_i \, ' \rangle}{\partial x_j} + \dfrac{\partial \langle u_j u_i \rangle}{\partial x_j} = -\dfrac{1}{\rho}\dfrac{\partial \langle p \rangle}{\partial x_i} + \upsilon \dfrac{\partial^2 \langle u_i \rangle}{\partial x_j \partial x_j} \\ \dfrac{\partial \langle u_i \rangle}{\partial x_i} = 0 \end{cases} \tag{1}$$

The Reynolds stress tensor can be expressed as follows Eq (2):

$$\tau_{ij} = \langle u_j \, 'u_i \, ' \rangle \tag{2}$$

The closure used on the Reynolds stress is based on the viscosity. This is to express the fact that the Reynolds constraint behaves with all the viscous constraints Eq (3):

$$\langle u_i \, 'u_j \, ' \rangle = -\upsilon_t \left(\frac{\partial \langle u_i \rangle}{\partial x_j} + \frac{\partial \langle u_j \rangle}{\partial x_i} \right) + \frac{2}{3}\delta_{ij} k \tag{3}$$

υ_t is the viscosity of the fluid and k is the instantaneous turbulent kinetic energy, we can write it as follows Eq (4):

$$k = \frac{1}{2}\langle u_i \, ' \rangle^2 \tag{4}$$

In the implementation of this model, the expression of Kolmogorov-Prandtl (ANSYS Fluent Theory Guide., 2013) concerning the turbulent viscosity is used Eq (5):

$$\upsilon_t = c_\mu \frac{k^2}{\varepsilon} \tag{5}$$

$$\frac{\partial k}{\partial t} + u_j \frac{\partial k}{\partial x_j} = -\langle u_i \, 'u_j \, ' \rangle \frac{\partial u_j}{\partial x_j} - \varepsilon + \frac{\partial}{\partial x_j}\left((\upsilon + \sigma_k \upsilon_t) \frac{\partial k}{\partial x_j} \right) \tag{6}$$

$$\frac{\partial \varepsilon}{\partial t} + u_j \frac{\partial \varepsilon}{\partial x_j} = -C_{\varepsilon 1} \langle u_i \, 'u_j \, ' \rangle S_{ij} \frac{\varepsilon}{k} - C_{\varepsilon 2} \frac{\varepsilon^2}{k} + \frac{\partial}{\partial x_j}\left((\upsilon + \sigma_\varepsilon \upsilon_t) \frac{\partial \varepsilon}{\partial x_j} \right) \tag{7}$$

where,

$S_{ij} = \frac{1}{2}\left(\frac{\partial \langle u_i \rangle}{\partial x_j} + \frac{\partial \langle u_j \rangle}{\partial x_i} \right)$ Is the average speed of the strain tensor

Cμ, Cε1, Cε2, σk, σε are adjusted constants of our model. They are determined by experiments on fundamental flows (turbulence grids, chiseled flow ...) and given in the following table.

Table 1: Constants of k-ε model

C_μ	$C_{\varepsilon 1}$	$C_{\varepsilon 2}$	σ_k	σ_ε
0.09	1.44	1.92	1.0	1.3

3.3 Numerical results

The surface distribution of the velocity in the x-y plane of the T-mixer is shown in (Figure 6). Indeed, the velocity increases suddenly from the impact of the two inlet fluids as shown by two red zones, where it attains its maximum value correspondent to the minimum values of the static pressure. The local pressure in the red zones was calculated, as a function of the Reynolds number of injected fluids in the inlet tubes of the T-mixer. This result, shown in (Figure 7), allows numerically defining the Reynolds number from which cavitation installs in the T-mixer.

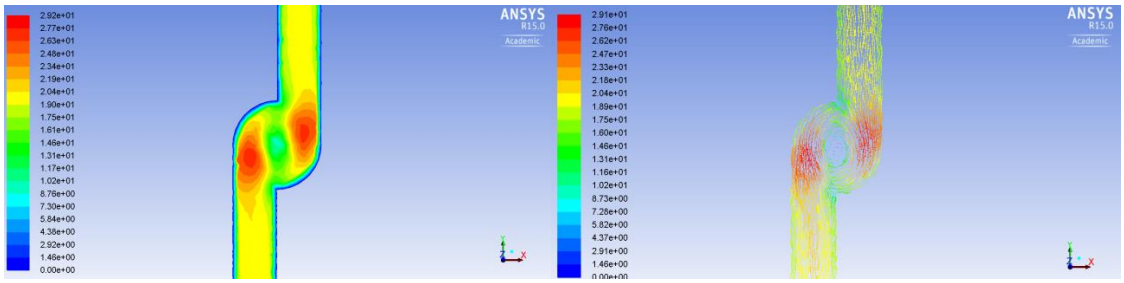

Figure 6: velocity fields and Current line (Re=8000)

The calculation of the vortex pressure presented in (Figure 7), has taken into account the liquid-gas interface pressure, which is cancelled in the single-phase liquid water flow but becomes significant in the biphasic fluid containing vapor phase. According to Herbert et al. (Herbert et al., 2006), the negative pressure *P'*<0 contributes to the centrifugal flow according to Eq. 8:

$$P = P_0 - 1/2\ \rho\omega^2 r^2 + P' \qquad (8)$$

Where P_0 is the pressure outside the tube, ρ is the water density, ω is the angular velocity and r is the distance between the center and the liquid-gas interface.

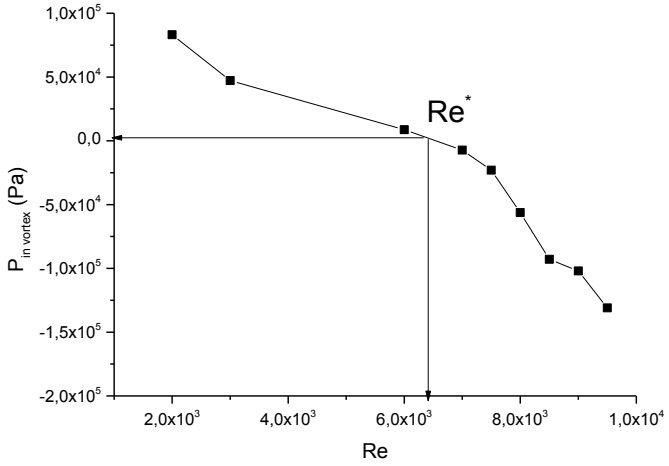

Figure 7: Pressure as a function of the Reynolds number at the inlet

The cavitation pressure is P_{vap} = 4000 Pa at 20 °C depicted in (Figure 7) was obtained from the Clapeyron equation (Wexler et al., 1976). As can be seen, our flow reaches the cavitation pressure about Re≈7000. By increasing the Reynolds number, it was found that the pressure further decreased to negative values.

4. Conclusions

In the present work, we report on hydrodynamics studies of a water flow through T-mixer with exocentric inputs. The SLS method was used to characterize the mass density perturbations in the flowing liquid. The abrupt increase of the scattered light intensity was observed at Reynolds numbers Re ≥ 7500 due to the appearance of the cavitation bubbles. The experimental observation of the cavitation threshold is supported with the results of CFD simulation of the velocity field and pressure drop in the T-mixer.

Reference

ANSYS Fluent Theory Guide, Release V15.0, November 2013

Azouani R., Mokrani L., Benmami M., Chhor K., Bocquet J.-F., Vignes J.-L., Kanaev A., 2007a, Preparation and chemical deposition of pure and doped TiO_2 sols: application to nanocoatings for reactive gas cleaning, Chem. Eng. Trans., 11, 77-82.

Azouani R., Soloviev A., Benmami M., Chhor K., Bocquet J-F, Kanaev A., 2007b, Stability and growth of titanium-oxo-alcoxy TixOy(OiPr)z clusters, J. Phys. Chem. C, 111 16243-16248.

Azouani R., Michau A., Hassouni K., Chhor K., Bocquet J-F., Vignes J-L., Kanaev A., 2010, Elaboration of pure and doped TiO2 nanoparticles in sol-gel reactor with turbulent micromixing:application to nanocoatings and photocatalysis, Chem. Eng. Res. Des., 88 1123-1130.

Cerutti S., Omar M.K., KATZ J., 2000, Numerical study of cavitation inception in the near field of an axisymmetric jet at high Reynolds number, Phys. Fluids, 12(10), 2444-2460.

Gaikwad V., Ranade V., 2016, Disinfection of water using vortex diode as hydrodynamic cavitation reactor, Asian J. Chem., 288 1867-1870.

Gavaises M., 2015, Visualisation and les simulation of cavitation cloud formation and collapse in an axisymmetric geometry. Int. J. f Multiphase Flow, 68, 14-26.

Gradl J., Schwarzer H.-C., Schwertfirm F., Manhart M., Peukert W., 2006, Precipitation of nanoparticles in a T-mixer: Coupling the particle population dynamics with hydrodynamics through direct numerical simulation, Chem. Eng. Process., 45, 908-916.

Herbert E., Balibar S., Caupin F., 2006, Cavitation pressure in water, Phys. Rev. E, 74, 041603.

Hosni M., Farhat S., Ben Amar M., Kanaev A., Jouini N., 2015, Mixing strategies for zinc oxide nanoparticle synthesisvia a polyol process, AIChE, 61, 1708-1721.

Knapp R.T., Daily J.W., Hammit F.G., 1970, Cavitation. Ed. McGraw-Hill Book Co., Inc., NY, USA.

Labidi S., Jia Z., Ben Amar M., Chhor K., Kanaev A., 2015, Nucleation and growth kinetics of zirconium-oxo-alkoxy nanopparticles, Phys. Chem. Chem. Phys., 17, 2651-2659.

Launder B-E., Spalding D-B., 1972, Mathematical models of turbulence, London: Academic Press Inc. (London) Limited.

Marchisio L., Rivautella L., Barresi A., 2006, Design and scale-up of chemical reactors for nanoparticle precipitation, AIChE, 52, 1877-1887.

Pandare A., Ranade V., 2015, Flow in vortex diodes, Chem. Eng. Res. Des., 102, 274-285.

Reynolds O., 1895, On the Dynamical Theory of Incompressible Viscous Fluids and the Determination of the Criterion, Philosoph. Trans. Roy. Sci. London, 186, 123-164.

Rivallin M., Benmami M., Kanaev A., Gaunand A., 2005, Sol-gel reactor with rapid micromixing modelling and measurements of titanium oxide nano-particle growth, Chem. Eng. Res. Des., 83 (A1), 1-8.

Salvador P., 2007, Numerical modeling of cavitating flows for simple geometries using Fluent V6.1 G.

Singhal A. K., Athavale M. M., Huiying L., Jiang L., 2002, Mathematical bases and validation of the full cavitation model. J. Fluids Eng., 124, 617-624.

Schwarzer, H-C., Peukert, W., 2004, Combined Experimental / Numerical Study on the Precipitation of Nanoparticles. AIChE J., 50 (12), 3234-3247

Wexler A., 1976, Vapor pressure formulation for water in range 0 to 100 °C. A revision, 1976, J. Res. Phys. Chem., 1 (5, 6).